Kinematic and paleomagnetic restoration of the Semail ophiolite (Oman) reveals subduction initiation along an ancient Neotethyan fracture zone

Douwe J.J. van Hinsbergen [a,*], Marco Maffione [a,b], Louise M.T. Koornneef [a,c], Carl Guilmette [d]

[a] *Department of Earth Sciences, Utrecht University, Heidelberglaan 2, 3584 CS Utrecht, Netherlands*
[b] *School of Geography, Earth and Environmental Sciences, University of Birmingham, B15 2TT, UK*
[c] *School of Geography, Earth and Environmental Sciences, Plymouth University, Drake Circus, PL4 8AA Plymouth, UK*
[d] *Département de Géologie et de Génie Géologique, Université Laval, Québec, QC G1K 7P4, Canada*

A B S T R A C T

The archetypal Semail ophiolite of Oman has inspired much thought on the dynamics of initiation of intra-oceanic subduction zones. Current models invoke subduction initiation at a mid-oceanic ridge located sufficiently close to the Arabian passive margin to allow initiation of continental subduction below the ophiolite within ∼10–15 Myr after the 96–95 Ma age of formation of supra-subduction zone crust. Here, we perform an extensive paleomagnetic analysis of sheeted dyke sections across the Semail ophiolite to restore the orientation of the supra-subduction zone ridge during spreading. Our results consistently indicate that the ridge was oriented NNE–SSW, and we infer that the associated trench, close to the modern obduction front, had the same orientation. Our data are consistent with a previously documented ∼150° clockwise rotation of the ophiolite, and we reconstruct that the original subduction zone was WNW-ward dipping and NNE–SSW striking. Initial subduction likely occurred in the ocean adjacent and parallel to a transform margin of the part of the Arabian continent now underthrust below Iran that originally underpinned the nappes of the Zagros fold-thrust belt. Subduction thus likely initiated along an ancient, continental margin-parallel fracture zone, as also recently inferred from near-coeval ophiolites from the eastern Mediterranean and NW Arabian regions. Subduction initiation was therefore likely induced by (WN)W–(ES)E contraction and this constraint may help the future identification of the dynamic triggers of Neotethyan subduction initiation in the Late Cretaceous.

© 2019 Elsevier B.V. All rights reserved.

1. Introduction

Subduction initiation is a critical step in the plate tectonic cycle, and how and where subduction zones form has therefore been at the forefront of geodynamic research for decades (e.g., Guilmette et al., 2018; Hall et al., 2003; Stern and Gerya, 2018). Ophiolites, i.e. exposed fragments of oceanic lithosphere that are often found thrust upon continental margins, have played a central role in the development of concepts of subduction initiation (Pearce et al., 1984; Stern et al., 2012). First, Pearce et al. (1984), among others, recognized that most ophiolites contain geochemical evidence that indicate formation at a spreading center located above a subduction zone (for this reason called supra-subduction zone (SSZ) ophiolites). Second, many SSZ ophiolites are associated

with metamorphic soles – typically high-temperature, low to high-pressure metabasalts and metasediments that are found below the ophiolite's mantle section, thought to have been derived from the top of now-subducted oceanic lithosphere. Their high metamorphic temperatures are atypical for mature, cool subduction zones and metamorphic soles are therefore thought to form at the plate contact during subduction zone infancy (e.g., Agard et al., 2016; Boudier et al., 1988; Guilmette et al., 2018; Hacker and Gnos, 1997; Pourteau et al., 2019; Soret et al., 2017; van Hinsbergen et al., 2015; Wakabayashi and Dilek, 2003). Because both the upper plate – the ophiolite – and the downgoing plate in these systems are oceanic, as deduced from oceanic lithologies in the metamorphic soles and underlying subduction mélanges, SSZ ophiolites are thought to result from intra-oceanic subduction initiation (Agard et al., 2007; Stern et al., 2012; van Hinsbergen et al., 2015; Wakabayashi and Dilek, 2003).

Models of intra-oceanic subduction initiation logically point at pre-existing weakness zones within oceanic lithosphere as loca-

---

* Corresponding author.
  E-mail address: d.j.j.vanhinsbergen@uu.nl (D.J.J. van Hinsbergen).

tions where subduction zones may form, either spontaneously or induced (e.g., Agard et al., 2007; Guilmette et al., 2018; Stern et al., 2012), at or near active intra-oceanic plate boundaries: transform faults or young fracture zones, ridges, or ridge-parallel detachment faults (Agard et al., 2007; Boudier et al., 1988; Duretz et al., 2016; Hall et al., 2003; Maffione et al., 2015a; Stern et al., 2012; van Hinsbergen et al., 2015).

Along the northern margin of Arabia, and as the highest structural unit in a microcontinent-derived fold-thrust belt in the eastern Mediterranean region, a discontinuous, ∼4000 km-long belt of SSZ ophiolites is found with well-constrained crustal ages of ∼96–90 Ma (Maffione et al., 2017; Rioux et al., 2016). The best-exposed and most complete of these is the Semail ophiolite of Oman, which has allowed mapping out 100's of km long, coherent fossil ocean floor (e.g., Nicolas et al., 2000). This ophiolite has inspired much thought on the process of subduction initiation and is widely considered to have formed in the incipient stages of an intra-oceanic subduction zone.

Given the overall ∼N–S long-term Arabia-Eurasia plate convergence, subduction is widely assumed to have formed along an ∼(WN)W–(ES)E striking mid-ocean ridge within the Neotethys (e.g., Duretz et al., 2016). As drivers for subduction initiation a far-field driven Arabia-Eurasia convergence rate increase of 2–3 cm/yr (Agard et al., 2007) was for instance proposed. Geological data, however, appear to challenge this assumption. Paleomagnetic constraints from sediments and igneous rocks of the ophiolite indicate that the Oman ophiolite underwent a major, clockwise vertical axis rotation of as much as 150° (e.g., Perrin et al., 2000; Morris et al., 2016). Back-rotating the present-day obduction front (as a proxy for the intra-oceanic trench location) according to these data suggests that the spreading center at which the Oman crust was formed had a (N)NE–(S)SW orientation, hence near-orthogonal to the Arabian passive-margin, not parallel to it. In addition, the earliest metamorphism of Arabian passive continental margin rocks found below the Oman ophiolite is dated at ∼80–85 Ma old (Warren et al., 2005), i.e. the Arabian passive margin was already buried at the trench as little as ∼10 Myr after SSZ ophiolite formation. This suggests that subduction initiated close to the Arabian passive margin, as also indicated by paleomagnetic paleolatitudes (Perrin et al., 2000). A Cretaceous mid-ocean ridge close to the Arabian passive margin, as commonly assumed in numerical and analogue models (e.g., Agard et al., 2014; Duretz et al., 2016) would be surprising: Opening of the Neotethys ocean and formation of the Arabian passive margin occurred in the Permian, as much as ∼170 Myr prior to Cretaceous subduction initiation (e.g., Béchennec et al., 1990; Stampfli and Borel, 2002). The presence of a Cretaceous mid-ocean ridge close to a Permian passive margin is unlikely, particularly since the original Neotethyan mid-oceanic ridge must have already subducted below the Eurasian margin in Jurassic time (Maffione et al., 2017; Stampfli and Borel, 2002).

In this paper, we provide the first paleomagnetic dataset from the sheeted dyke sections of the Oman ophiolite to kinematically restore the orientation of its SSZ spreading ridge during subduction zone infancy. To this end, we collected a large paleomagnetic data set from ten localities in sheeted dyke sections along the strike of the Oman ophiolite to determine through net tectonic rotation analysis the original orientation of the sheeted dykes. We then place the Oman ophiolite in plate kinematic context using the configuration of the Arabian passive margin restored for continental subduction in the Zagros mountains (McQuarrie and van Hinsbergen, 2013), cast in a paleomagnetic frame of reference (Torsvik et al., 2012). Finally, we discuss the implications for the tectonic setting and nature of the weakness zone that facilitated Oman's subduction initiation, and search for settings in today's snapshot of plate tectonic history that may provide analogues.

2. Geological setting

The Semail ophiolite in Oman consists of a large, well-preserved oceanic lithosphere nappe containing an estimated 4–7 km thick crustal sequence, and a 8–12 km thick mantle sequence (e.g., Nicolas et al., 2000). The ophiolitic sequence displays a Penrose pseudostratigraphy composed from top to bottom of a sedimentary cover (radiolarian cherts), volcanics (pillow lavas and lava flows), sheeted dykes, isotropic and layered gabbros, peridotites (harzurgites and dunites), and a 300–500 m thick metamorphic sole with an inverted metamorphic grading (e.g., Cowan et al., 2014; Hacker, 1991; Nicolas et al., 2000; Searle and Cox, 1999; Soret et al., 2017). The ophiolite overlies a sequence of deep-marine, Permian to Cretaceous sediments interpreted to be derived from the distal Arabian margin or the adjacent oceanic crust – the Hawasina nappes – and underlying Arabian margin-derived nappes (Béchennec et al., 1990).

In the northern part of the ophiolite, the extrusive sequence is geochemically layered (Ernewein et al., 1988; Nicolas et al., 2000). Basalts with a geochemistry similar to mid-ocean ridge basalts (N-MORB) dominate in the lower part of the volcanic sequence, called *Geotimes Unit* or *Unit V1* by Ernewein et al. (1988). Above this unit are the Lasail and Alley volcanic suites, collectively termed *Unit V2* by Ernewein et al. (1988), which consist of depleted arc tholeiites and boninites interpreted as products of hydrous melting of a previously depleted mantle source (e.g., Godard et al., 2006). This geochemical pattern in the crustal sequence of the Oman ophiolite led to the formulation of different tectono-magmatic models invoking formation either in an open ocean (e.g., Nicolas, 1989) or above an active subduction zone (e.g., Pearce et al., 1984). A more recent study, however, suggested that the Geotimes MORBs may have been produced under high water content, hence more likely above an incipient subduction zone (MacLeod et al., 2013).

Paleomagnetic data from the extrusive sequence of the Semail ophiolite indicate a rigid block clockwise (CW) rotation up to ∼150° in the northwestern segment of the ophiolite (north of the Hawasina tectonic window), and only minor counterclockwise (CCW) rotations up to ∼20° in the southeastern portion of the ophiolite (Feinberg et al., 1999; Perrin et al., 2000; Weiler, 2000). This was originally interpreted as the result of major relative rotations between the northern and southern part of the ophiolite (Nicolas et al., 2000; Perrin et al., 2000), until Feinberg et al. (1999) and Morris et al. (2016) documented the occurrence of a pervasive remagnetization of the ophiolite in the southern segment, which occurred during or soon after the emplacement of the ophiolite above the Arabian continental margin, in the Late Cretaceous (e.g., Nicolas et al., 2000; Searle and Cox, 1999; Searle et al., 2004). In particular, Morris et al. (2016) suggested that the minor CCW rotation of the southern block occurred after the remagnetization event and reflects only the latest stages of motion of the ophiolite relative to Arabia.

Zircon U–Pb dating of the plutonic section of the Semail ophiolite indicates that the ophiolitic crust formed at a fast spreading ridge in less than ∼1 Ma in the Late Cretaceous (∼96–95 Ma; Rioux et al., 2016), only just preceding other Neo-Tethyan ophiolites from Turkey and Cyprus with 94–90 Ma ages (e.g., Maffione et al., 2017). Zircon U–Pb and hornblende and mica Ar–Ar ages from garnet-bearing metamorphic sole rocks are similar or slightly younger than the magmatic sequence (96.2–92.6 Ma; Hacker et al., 1996; Rioux et al., 2016; Warren et al., 2005), indicating cooling and exhumation of the sole synchronous with upper plate spreading and formation of the ophiolitic crust (e.g., van Hinsbergen et al., 2015). More recently, garnet Lu–Hf ages from the uppermost, garnet-bearing layer of the metamorphic sole in Oman have constrained subduction-related prograde metamorphism at 104 Ma (Guilmette et al., 2018) and a nearly identical Lu/Hf age
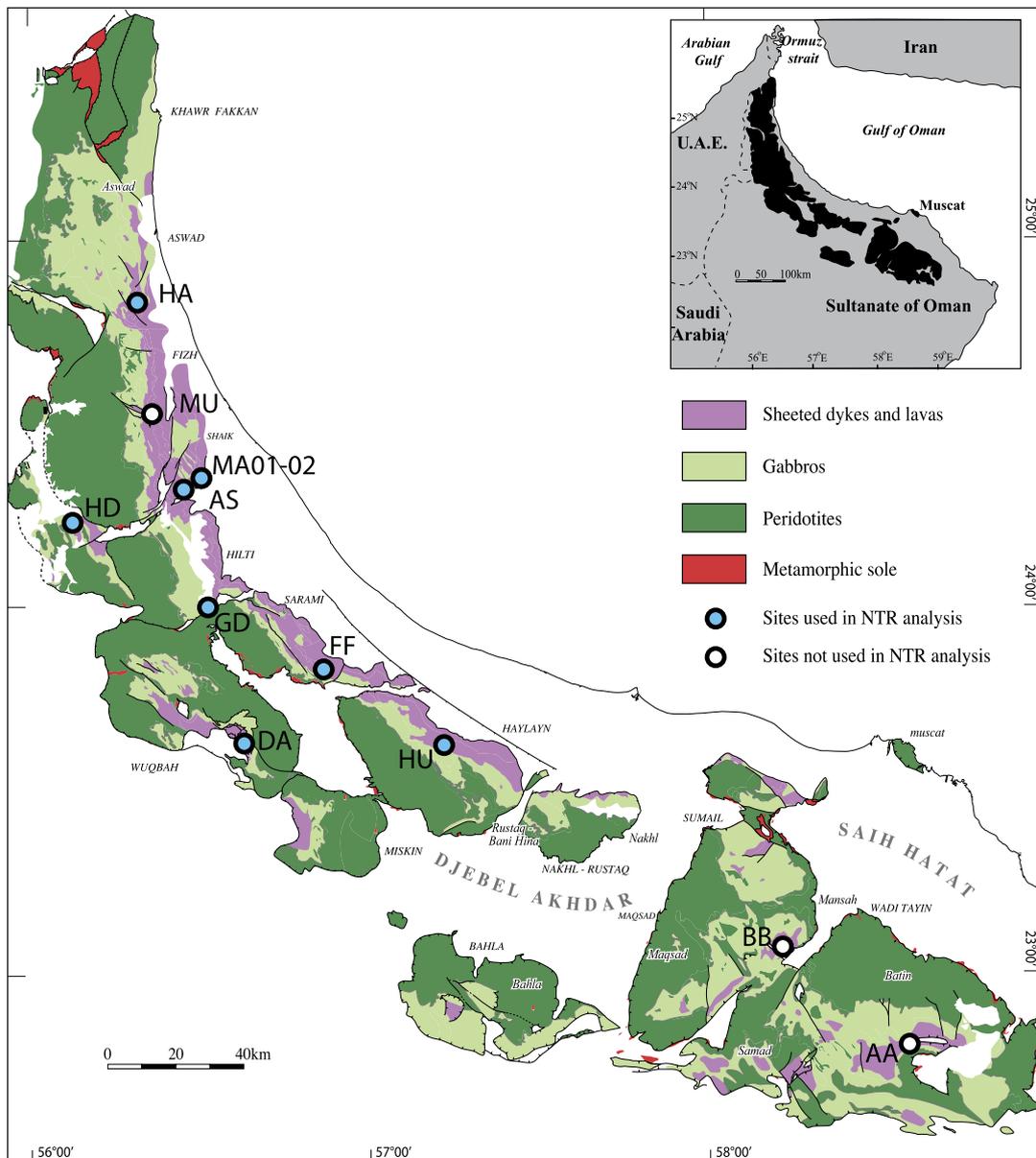
Fig. 1. Geological map of the Oman ophiolite.

was reported from Turkey (Pourteau et al., 2019), indicating near-synchronous timing of subduction initiation. According to these new results, upper plate spreading (and ophiolite formation) post-dated the initiation of subduction by ~8–12 Ma. Because spontaneous subduction initiation requires initial slab roll-back and simultaneous upper plate extension (Stern et al., 2012), this delay demonstrates that subduction initiation must have been induced (Guilmette et al., 2018), i.e. triggered by a far-field tectonic stress.

3. Sampling and methods

A total of 380 standard paleomagnetic samples were collected from 12 localities, 10 within the sheeted dyke section and two in the extrusive sequence (Fig. 1). All sampled dykes were fresh, lacked any indication for pervasive ductile or brittle deformation, and showed the typical grading for sheeted dyke sequences, from coarser-grained on one end to a finer-grained, chilled margin on the other. All samples were drilled in the field using a water-cooled portable rock drill and were oriented *in situ* using both magnetic and sun compasses. Mean paleomagnetic directions for each sam-

pling site were calculated by averaging characteristic remanent magnetizations (ChRMs) interpreted from typically 20–50 samples collected from six to eleven adjacent chilled margin-bearing dykes. Orientation of the volcanic sequence at two sites was determined using the primary layering of pillow lavas and an intercalated lava flow unit.

The nature of the magnetic carriers was characterized through rock magnetic experiments and thin section analysis carried out at the paleomagnetic laboratory 'Fort Hoofddijk' at Utrecht University (Netherlands). High-temperature thermal variation of the magnetic susceptibility was investigated via heating-cooling cycles from room temperature to 700 °C in argon atmosphere using a KLY-3 Kappabridge (AGICO) coupled with a CS3 apparatus. The Curie temperatures were determined from the thermal demagnetization results. Hysteresis parameters were calculated through hysteresis loops with peak fields of 0.6–1.5 T, using an alternating gradient magnetometer (Micromag AGM, Princeton). Mineralogical assemblages and the nature and distribution of the ferromagnetic minerals were determined by analyzing polished thin sections under both transmitted light and scanning electron microscope (JEOL

JCM-6000), and by carrying out elemental analysis with an energy-dispersive X-ray (EDX) analyzer coupled with the SEM.

Remanence components were analyzed using mainly stepwise alternating field (AF) demagnetization with variable increment steps from 5 to 100 mT. About 10% of the samples were also demagnetized thermally in a magnetically shielded furnace (ASC, TD48-SC) using variable increment steps from 100° to 580 °C (or until complete demagnetization). AF demagnetization and measurement of the remanence after each demagnetization step were conducted using a robotized superconducting (SQUID) cryogenic magnetometer (Mullender et al., 2016) located in a magnetically shielded room. Demagnetization data were plotted on orthogonal diagrams (Zijderveld, 1967) and the remanence components were isolated via standard principal component analysis (Kirschvink, 1980) using the online software package www.paleomagnetism.org (Koymans et al., 2016). ChRM components with maximum angular deviation (MAD) larger than 10° were discarded from further analysis. Site mean ChRM directions were computed using Fisherian statistics (Fisher, 1953) on virtual geomagnetic poles (VGPs) associated to the isolated ChRMs, and after having applied a fixed 45° cutoff to the VGPs.

The computed site mean directions were then used to calculate the tectonic rotations at each site using a net tectonic rotation approach (Allerton and Vine, 1987). This technique prevents possible biases associated with classic tilt correction in units lacking paleohorizontal constraints, like sheeted dykes, and has been successfully applied to other ophiolites (e.g., Maffione et al., 2017; Morris et al., 1998). Rather than decomposing the deformation into a tilt and a vertical axis rotation component, a net tectonic rotation analysis computes the single rotation around an inclined axis that restores both the rock unit to its original orientation (i.e., vertical for sheeted dykes) and the measured *in situ* remanence to a selected reference direction. The reference direction is the direction of the magnetic field at the time and latitude at which the remanence was acquired. The declination of the reference direction is inferred from the geocentric axial dipole (GAD) hypothesis (i.e., the time-averaged declination of the magnetic field points towards the geographic north pole) and is therefore D = 000°. The inclination of the reference direction has been calculated by combining all the existing (not remagnetized) paleomagnetic data from the layered gabbros and the extrusive sequence (Perrin et al., 2000; Shelton, 1984; Weiler, 2000), including the results from the two pillow basalt sites in this study. The tilt corrected mean inclination calculated from this dataset, representing the inclination of the reference direction, is 21.5° ± 6.6° (Fig. S1).

A set of net tectonic rotation solutions is expressed as (i) azimuth and plunge of the rotation axis, (ii) magnitude and sense of the rotation, and (iii) initial strike of the unit. When applied to vertical units like dykes, two permissible sets of net tectonic rotation solutions are obtained if the dykes can be restored to the vertical. In this case, three selection criteria are used to choose the preferred solution at each site: (1) the calculated rotation has to restore the units to their current position (e.g., a solution yielding overturned beds when units are just gently dipping should be discarded); (2) both the rotation sense and magnitude have to be consistent with the known regional and/or local deformation pattern; (3) multiple sites within a relatively small area have to show similar net tectonic rotation parameters (assuming local rotations are minor).

One set of solutions is instead obtained when dykes are not restored to vertical (e.g., because they did not intrude vertically). Single solutions are geologically meaningless and should be discarded as both the initial dyke orientation and the rotation parameters will only depend on the orientation of the reference direction (e.g., the initial dyke orientation will always strike perpendicular to the reference direction, hence will always be E–W).

Once a preferred solution has been chosen, an iterative net tectonic rotation analysis (Morris et al., 1998; Koymans et al., 2016) is then used to model the uncertainties on the reference direction (only its inclination), the site mean direction, and the dyke orientation. This routine within the net tectonic rotation analysis package is available at www.paleomagnetism.org and produces at each site 75 permissible solutions per set of solutions (hence 150 when dykes are restored to vertical).

4. Results

4.1. Magnetic carrier analysis

Temperature variation of the magnetic susceptibility (Fig. 2) is irreversible, with susceptibility values being commonly lower after heating, hence showing mineralogical transformations induced by the experiments. These transformations did not produce new mineralogical phases, as the Curie temperatures for the heating and cooling curve are the same. On the other hand, in the pillow lavas (site MA01; Fig. 2) variable Curie temperatures are inferred from the heating and cooling paths. Curie temperatures of 570–580 °C are observed within the dyke samples (Fig. 2), indicating nearly pure magnetite as magnetic carrier (Dunlop and Özdemir, 1997). Sites DA and HA show additional Curie temperatures between 300° and 330° (Fig. 2), which is consistent with a minor occurrence of iron sulphides, likely pyrrhotite. If present, the break-down of iron sulphides expected during heating at ∼500 °C (Dunlop and Özdemir, 1997) did not produce any new magnetite as our experiments were conducted in argon atmosphere, hence in reducing conditions. This would explain the lower susceptibility values of the cooling curves in all sites (except site AS where new magnetite might indeed have formed during the experiment; Fig. 2). The removal of iron sulphides during the heating is further supported by the absence of inflections in the cooling paths around 300–330° (Fig. 2). Site AS shows a slightly higher Curie temperature of 595 °C, suggesting the occurrence of partly oxidized (maghemitized) magnetite, common in mafic magmatic rocks (Dunlop and Özdemir, 1997). Pillow lavas from site MA01 show two Curie temperatures of ∼545 °C and ∼450 °C, compatible with the occurrence of both Ti-poor and Ti-rich titanomagnetite, respectively. Similar blocking temperatures have also been observed at all sites during the thermal demagnetization experiments, confirming the occurrence of magnetite, titanomagnetite, and (titano)maghemite as main carriers of the magnetization in the sampled dykes and lavas.

Relatively narrow to more open hysteresis loops characterize all the dyke samples (Fig. 3), indicating the predominance of pseudo-single-domain (PSD; 0.05–3 μm) and perhaps minor single-domain (SD; <0.05 μm) grains (Dunlop and Özdemir, 1997). On the other hand, pillow lava samples show very narrow hysteresis loops (Fig. 3), which are typically observed in rocks dominated by multidomain (MD; >3 μm) ferromagnetic grains (Dunlop and Özdemir, 1997).

Ten thin sections from both dykes and pillow lavas were analyzed. The main mineralogical assemblage in dykes is, in order of abundance, plagioclase, clinopyroxene, orthopyroxene, chlorite, and opaque minerals. In some dyke samples (sites AA and HU) opaque minerals are as large as 0.1–0.2 mm. Pillow lavas are much more weathered and altered than the dykes. The microscopic fabric of both dykes and pillow lavas is purely magmatic, with frequent euhedral plagioclase and pyroxene minerals (more commonly observed in dykes) forming a matrix with no internal fabric. The opaque minerals are also randomly dispersed within this matrix. Chlorite, which is always present in all the samples, occurs randomly dispersed within the isotropic matrix, suggesting a static metamorphism likely associated to seafloor hydrothermal alter-
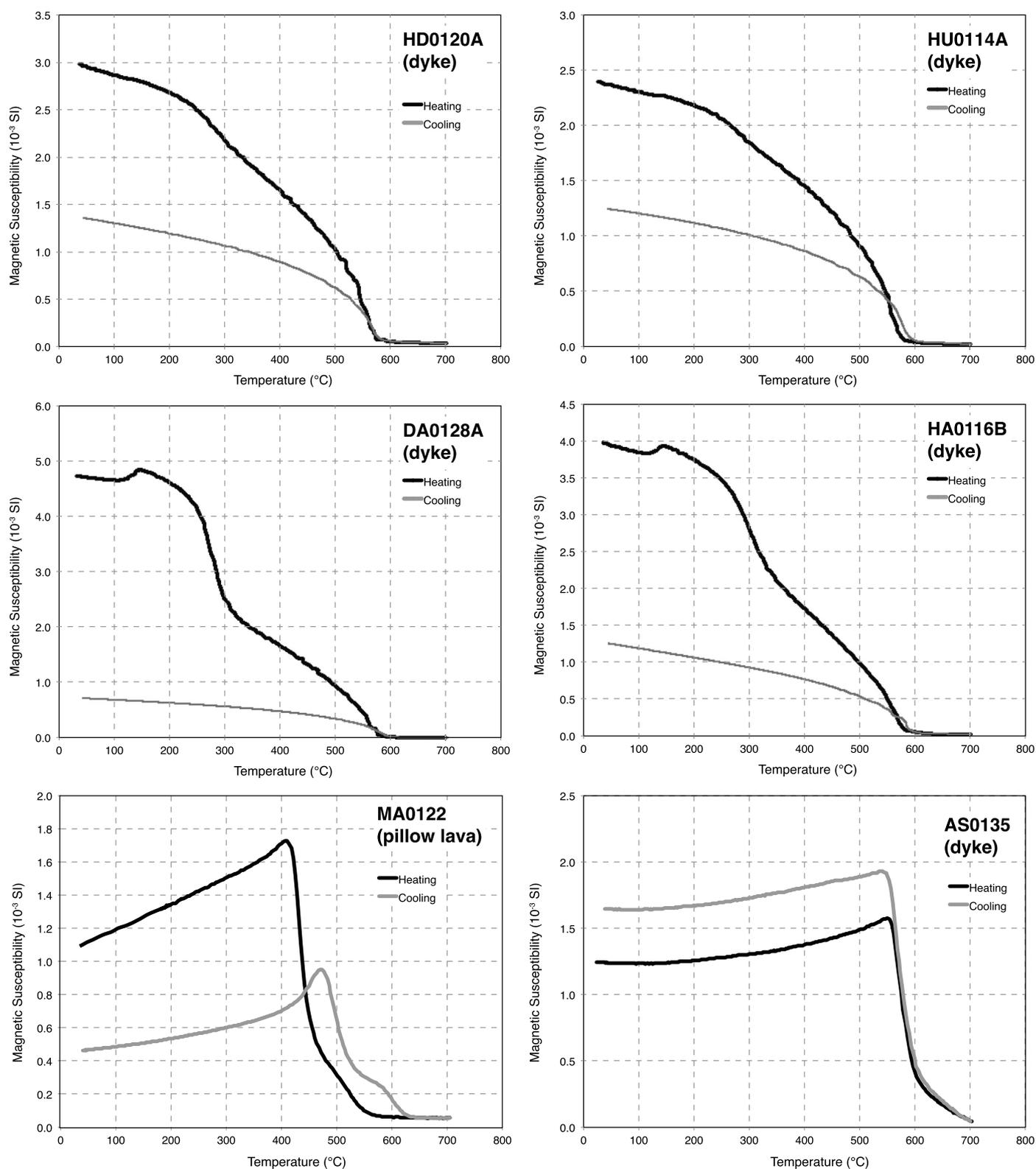
Fig. 2. High-temperature variations of low-field magnetic susceptibility (k) for six representative samples (five from dykes and one from pillow lavas). Diagrams are mainly irreversible, showing mineralogical transformation during heating. Curie temperatures have been inferred from the heating paths.

ation, as frequently observed in other ophiolites (e.g., Maffione et al., 2017). Such metamorphism occurs at very low temperatures and normally does not affect the magnetic remanence of rocks emplaced at a mid-ocean ridge.

SEM analysis and EDX characterization (Fig. 4), revealed the occurrence of angular magnetite and titanomagnetite, sometimes

with exolution lamellae, with grain sizes variable between 1 μm (pseudo-single-domain – PSD) and 100 μm (multidomain – MD). At few samples from sites FF and AS, iron- and titanium-rich oxides up to 1 mm in size and showing compositional bands have been observed and interpreted as ilmenite. This is supported by the fact that the magnetization of samples carrying such large il-
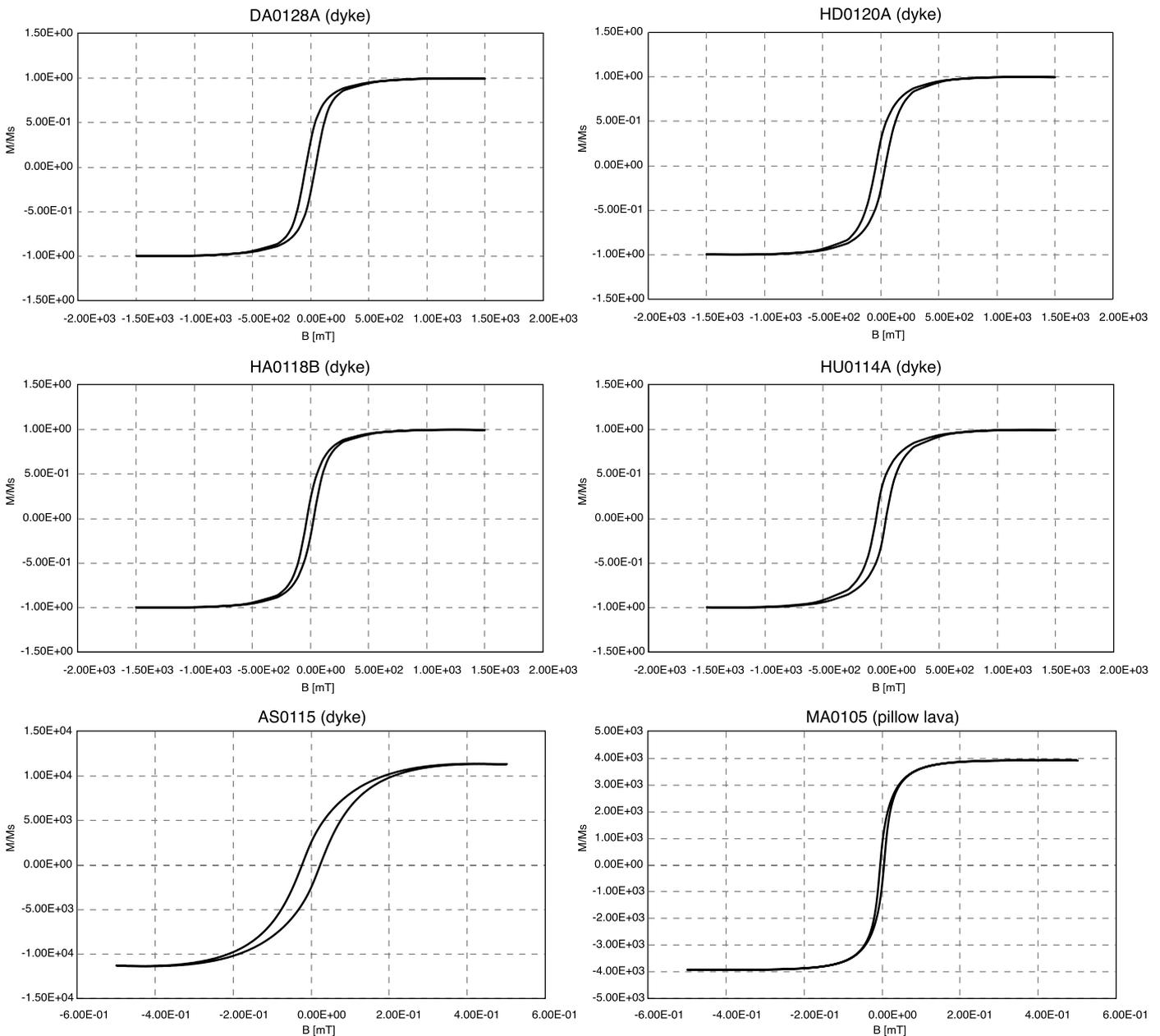
Fig. 3. Hysteresis loops for six representative samples (the same as in Fig. 2), showing predominantly narrow to slightly open loops typical of multidomain (MD) magnetic grains.

menite minerals (which is not magnetic) is comparable to that of other samples.

4.2. Paleomagnetic results

Natural remanent magnetization (NRM) intensity from 380 analyzed samples varies between several 10s of mA/m and 4 A/m, suggesting substantial variations in ferromagnetic mineral concentration across the sampled rocks. A total of 340 characteristic remanent magnetizations (ChRMs) were interpreted from the 380 analyzed samples, with the remaining 40 samples showing noisy, uninterpretable demagnetization diagrams, or MAD values above the chosen threshold of 10°.

AF demagnetization diagrams show two components of magnetization: a low-coercivity viscous component usually removed at 10–15 mT, and a stable high-coercivity component isolated within an interval between 20 and 100 mT (Fig. 5). At about half of

the samples, these high-coercivity components were isolated using great circle fitting (McFadden and McElhinny, 1988), which denoted the occurrence of high-coercivity phases that could not be removed at 100 mT. We suspect this effect might be associated with partial maghemitization of the original magnetite, which causes a slight increase of coercivity. Although this hypothesis remains a valid explanation for the remanence behavior, is not supported by thin section microscope analyses. This might be due to the fact that cracks associated with maghemitization of original (titano)magnetite can sometimes be difficult to identify in thin section.

Overall, AF demagnetization treatment was more effective in isolating the ChRM components (Fig. 5), and produced more stable demagnetization components compared to the thermal demagnetization technique (Fig. 5E). Nevertheless, the ChRM directions determined from both AF and thermally demagnetized twin specimens are fully consistent (Fig. 5C), suggesting that these are
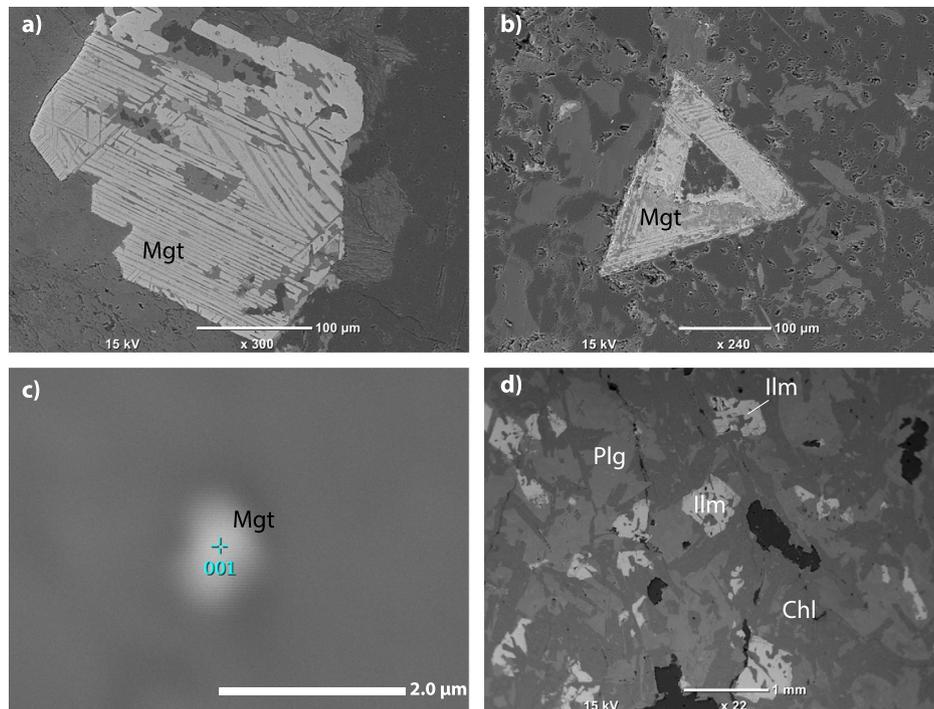
Fig. 4. Back-scattered electron (BSE) images of representative thin sections from sheeted dykes showing the presence of iron oxides (magnetite, titanomagnetite, and possibly ilmenite) with variable size from ~1 μm to ~1 mm.
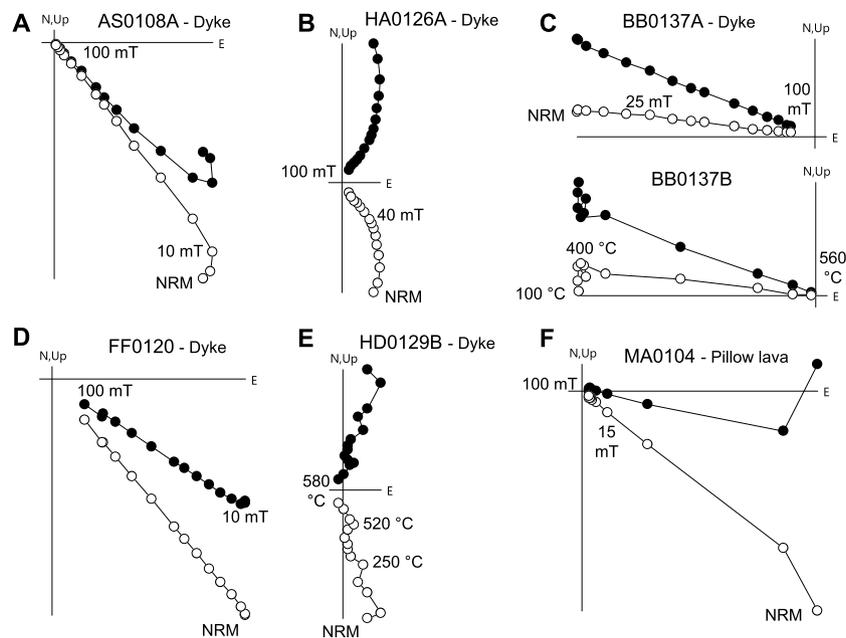

Fig. 5. A–F – Representative orthogonal vector plots (Zijderveld diagrams) of both alternating field and thermal demagnetization for various sites (in situ coordinates). C – An example of consistent ChRM directions acquired in AF and TH demagnetized sister samples. NRM = natural remanent magnetization. Steps are shown in °C or mT.

high-stability, likely primary remanence components suitable for tectonic interpretations.

Site mean directions (*in situ* coordinates) at 10 out of 12 sites (Fig. 6; Table 1) are significantly different from the present-day GAD field direction at the mean latitude of the Oman ophiolite (D/I = 000°/42°), hence ruling out any recent remagnetization. The remaining two sites (AA and MU) show northerly mean directions that are very close to the expected inclination of the present-day GAD, suggesting possible recent remagnetization (Fig. 6; Table 1). For now, this remagnetization cannot be confirmed based on this evidence alone and therefore we use all sites for the net tectonic

rotation analysis. At site HU, several ChRM directions that are close to the present-day GAD direction were discarded due to possible recent remagnetization before computing the site mean direction.

Besides sites AA and MU with northerly directions, the other ten sites show *in situ* site mean directions varying between southeastward, northeastward, and northwestward directions (Fig. 6; Table 1). The tilt-corrected mean direction from the two combined pillow lava sites (MA01 and MA02) has D = 093.4° and I = 15.9°, and indicates a vertical axis rotation of 93.4° CW (Table 1). This value is consistent with previous results (Morris et al., 2016; Perrin et al., 2000) showing E to SE-directed tilt-corrected rem-
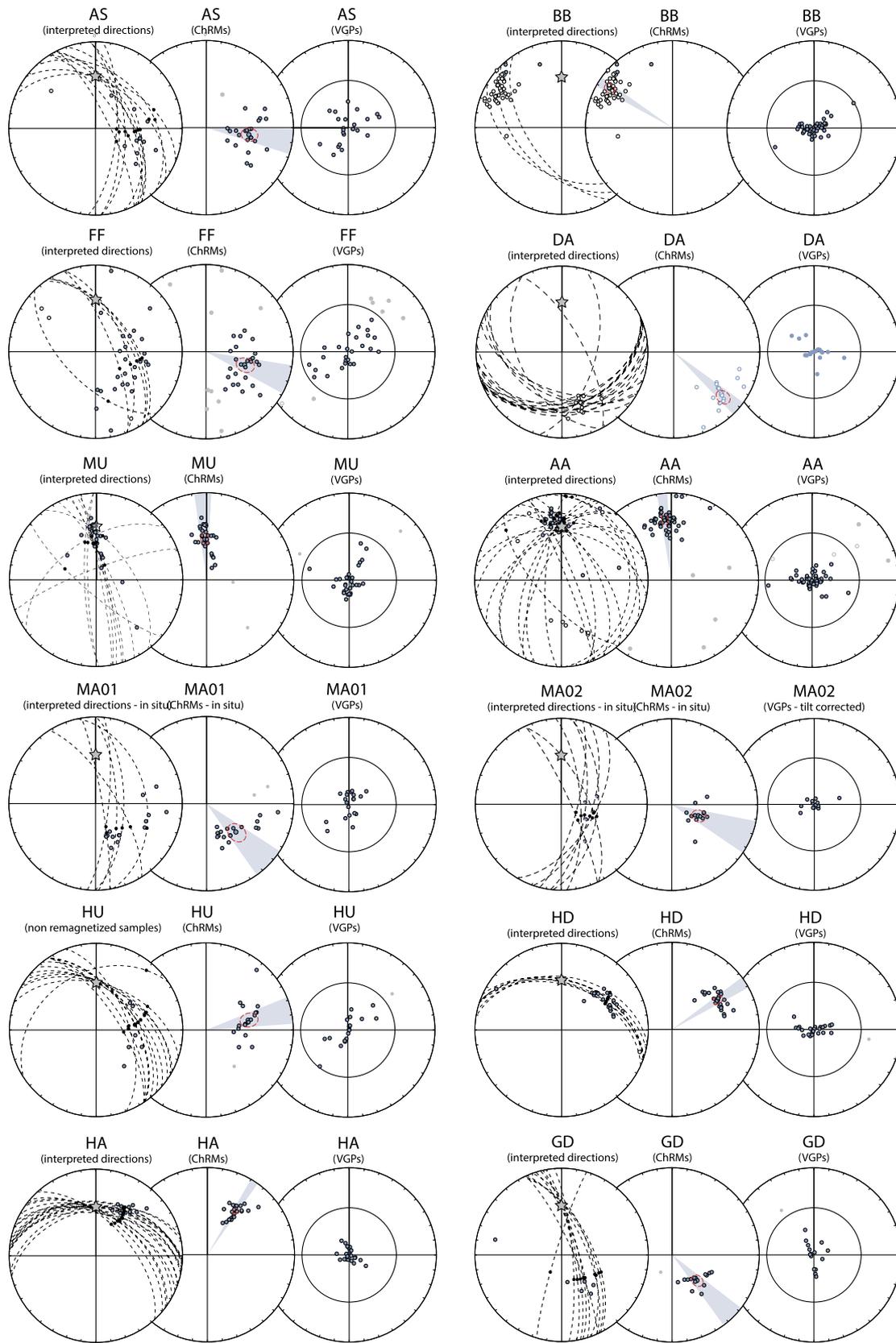
Fig. 6. Stereographic projections of the interpreted characteristic remanent magnetization directions (ChRMs) and virtual geomagnetic poles (VGPs) from all sites. The great circles used in the principal component analysis are shown in the left diagrams (dotted curve), together with the direction isolated from these (small black dots). The middle ChRM plots show all the ChRM directions calculated from best-fit lines and great circle analysis (blue dots = normal polarity; open dots = reverse polarity; gray dots = discarded direction after 45° cut-off). The red ellipse is the cone of confidence around the computed mean direction, while the light blue shaded area is the error on the mean declination (ΔD in Table 1). The VGP plots on the right of each site show the accepted VGPs (blue dots) and the discarded VGPs (gray dots), which in fact fall outside the solid inner circle that represents the 45° cut-off. The Grey star in the left plots is the present-day GAD field direction. (For interpretation of the colors in the figure(s), the reader is referred to the web version of this article.)

nance directions indicating large CW rotation of the whole ophiolite.

The primary nature of the isolated ChRMs cannot be assessed using classical fold tests due to the lack of paleohorizontal control in dykes (Allerton and Vine, 1987; Morris et al., 1998). Fold tests could not be performed on the two pillow lava sites either, as these rocks have similar orientations. VGP distribution has been demonstrated to be useful to assess whether a paleomagnetic data scatter may reflect paleosecular variation (PSV) of the paleomagnetic field, as would be expected if the directions were primary, or whether PSV is underrepresented or overrepresented, which may signal undersampling of PSV e.g. due to remagnetization, or local deformation or poorly resolved ChRM direction, respectively (Deenen et al., 2011). VGP scatters at all the sites except HA and is consistent with the expected scatter induced by paleosecular variation ($A_{95min} < A_{95} < A_{95max}$; Fig. 6 and Table 1). The scatter of ChRMs at site HA is smaller than that produced by secular variation (i.e., $A_{95} < A_{95min}$; Table 1). This may be because the majority of the remanence directions (i.e., 18 out of 30) at site HA have been computed using great circles analysis (McFadden and McElhinny, 1988). Although mathematically and statistically reliable, these directions do not necessarily replicate the natural scatter of the directions due to secular variation of the geomagnetic field.

As an extra first-order check on the primary origin of the remanence, we calculated the paleomagnetic direction after applying a straightforward tilt correction of the dykes to the vertical, assuming they tilted about a horizontal axis, and compare these directions to the declinations of the non-remagnetized and remagnetized parts of the ophiolite identified by Morris et al. (2016). Those authors showed that primary (tilt corrected) remanence components from the crustal sequence have an E-ward to SE-ward direction, while rocks remagnetized during the continental emplacement in the Late Cretaceous differ by ~100–170° and have a NNW direction instead. As explained in the Method section, it is unlikely that the sheeted dykes underwent a tilt about an exactly horizontal axis (which is why we applied a net tectonic rotation analysis (Allerton and Vine, 1987)), and the 'tilt-corrected' values in Table 2 are a crude estimate of the true vertical axis rotation, but given the major angular difference between the remagnetized and non-remagnetized directions identified by Morris et al. (2016), it is sufficient to test to which population the dyke directions isolated in our study belong. The tilt corrected directions at seven sheeted dyke sites (AS, DA, FF, HA, HU, GD) have declinations ranging from NE to SE, hence consistent with a primary origin of their remanence, whilst sites BB and AA, both from the southern sector of the ophiolite where major remagnetization events have been reported (Morris et al., 2016), show NW and NNW tilt corrected directions consistent with remagnetization. Based on the above evidence we interpret that remanence as primary at eight sites (with a small uncertainty for sites HD and MU) and therefore we use the computed mean directions at these sites for the net tectonic rotation analysis.

4.3. Net tectonic rotation analysis

Net tectonic rotation analysis of the eight sheeted dyke sites with a primary remanence succeeded in restoring both the dykes back to their original (vertical) orientation and the computed in situ paleomagnetic directions to the chosen reference direction, generating two sets of permissible solutions at each site (Table 2). Because the Oman ophiolite underwent an overall large (up to 150°) CW vertical axis rotation (see Morris et al. (2016) for a comprehensive review), preferred solutions were selected among those satisfying all the three criteria listed in the Methods section.

Preferred solutions could instead be selected at seven sites (Table 2). At sites AS, HA, and GD the preferred solutions are those

Table 1
Paleomagnetic results from the Oman Ophiolite.

Site	Lithology	Lat (N)	Long (E)	δDipDir (N meas.)	Dip dir.	Dip	ChRM interpr.	n/N	D	ΔDx	I	ΔIx	D_{TC}	I_{TC}	K	A_{95}	A_{95min}	A_{95max}
AS	SD	24°20′09″	56°28′36″	5.4 (9)	235	41	12 L + 12 GC	22/24	097.5	8.3	49.5	8.1	081.3	7.9	19.9	7.1	3.5	11.7
DA	SD	23°37′45″	56°38′06″	6.9 (8)	088	39	3 L + 18 GC	18/21	131.2	5.2	−27.1	8.5	126.6	12.6	40.7	5.0	3.6	12.0
FF	SD	23°49′38″	56°52′46″	6.0 (6)	255	54	29 L + 6 GC	26/35	108.8	9.9	51.4	9.1	096.6	19.1	12.5	8.4	3.3	10.5
HA	SD	24°48′29″	56°17′38″	5.7 (11)	026	48	12 L + 18 GC	30/30	032.7	2.7	40.4	3.4	060.7	81.0	115.7	2.5	3.1	9.6
HD	SD	24°13′40″	56°07′53″	3.2 (11)	096	65	21 L + 7 GC	26/28	057.3	4.0	38.1	5.4	037.0	55.0	58.2	3.7	3.3	10.5
HU	SD	23°37′14″	57°14′59″	3.5 (6)	098	79	7 L + 13 GC	19/20	077.0	9.0	49.0	9.0	070.8	59.1	19.4	7.8	3.7	12.8
GD	SD	23°59′04″	56°29′52″	3.8 (9)	234	60	6 L + 11 GC	15/17	135.7	8.1	56.5	6.2	102.3	43.0	35.8	6.5	4.1	14.9
*BB	SD	23°05′02″	58°10′39″	2.3 (6)	193	77	43 L + 3 GC	46/46	302.1	3.4	−15.9	6.4	298.1	−19.7	39.4	3.4	2.6	7.3
*AA	SD	22°48′36″	58°34′03″	7.5 (10)	073	71	35 L + 18 GC	48/53	354.0	3.5	31.1	5.3	342.1	32.8	39.2	3.3	2.6	7.2
*MU	SD	24°30′44″	56°21′13″	12.8 (8)	272	43	24 L + 12 GC	33/36	357.5	5.7	51.6	5.2	043.1	34.8	28.2	4.8	3.0	9.1
MA01[A]	PL	24°20′34″	56°30′27″	4.3 (6)	061	49	14 L + 6 GC	18/20	134.0	11.0	51.4	10.1	–	–	14.8	9.3	3.8	13.3
MA01[B]	PL	24°20′34″	56°30′27″	–	–	–	–	20/20	098.2	6.2	18.9	11.2	–	–	29.8	6.1	3.6	12.4
MA02[A]	PL	24°20′34″	56°30′27″	4.4 (6)	057	58	5 L + 8 GC	13/13	112.7	11.6	62.6	6.8	–	–	25.9	8.3	4.3	16.3
MA02[B]	PL	24°20′34″	56°30′27″	–	–	–	–	13/13	086.6	5.1	11.4	9.9	–	–	66.9	5.1	4.3	16.3
MA01/02[A]	PL	24°20′34″	56°30′27″	–	–	–	19 L + 14 GC	32/33	124.7	9.2	56.5	7.0	–	–	13.1	7.3	3.0	9.2
MA01/02[B]	PL	24°20′34″	56°30′27″	–	–	–	–	33/33	093.4	4.5	15.9	8.5	–	–	32.0	4.5	3.0	9.1

* Remagnetized sites. [A] In situ directions. [B] Tilt corrected directions. Lithologies are sheeted dykes (SD) and pillow lavas (PL), δDipDir is the 95% confidence around the mean direction. ChRM interpretation has used best-fit lines (L) and great circles (GC) fitting. n/N is the number of dykes measured in the field. (N meas.) is the number of dykes measured in the field to calculate the mean direction. ChRM interpretation has used best-fit lines (L) and great circles (GC) fitting. n/N is the number of specimens used in the statistics over the total number of analyzed samples. D, dDx, I, dIx are declination and associated error, and inclination and associated error. D_{TC} and I_{TC} are the tilt corrected calculated for the dykes using the classic tilt correction method (restoring the dykes to vertical). Note that these are for first-order comparison with primary and remagnetized directions identified by Morris et al. (2016) only, and give approximate rotation only. α_{95} = semiangle of the 95% cone of confidence around the site-mean ChRM direction (Fisher, 1953). K is Fisher's precision parameter relative to the ChRMs (Fisher, 1953). A_{95} is the semiangle of the 95% cone of confidence around the mean virtual geomagnetic pole (VGP). K is Fisher's precision parameter relative to the VGPs. A_{95min} and A_{95max} are the minimum and maximum semiangle of the 95% cone of confidence expected for the given dataset by paleosecular variation.

Table 2
Net tectonic rotation solutions from the sheeted dykes of the Oman ophiolite.

Site	Preferred solution						Alternate solution					
	Rotation axis		Rotation		Initial dyke		Rotation axis		Rotation		Initial dyke	
	Azimuth	Plunge	Magnitude	Sense	Strike	Dip	Azimuth	Plunge	Magnitude	Sense	Strike	Dip
AS	253.8	40.4	78.5	CW	072.6	90	054.0	11.0	105.6	CCW	107.4	90
DA	131.8	61.4	135.5	CW	055.0	90	227.8	32.5	157.3	CW	125.0	90
FF	287.5	65.3	97.4	CW	070.8	90	246.1	11.2	089.3	CW	109.2	90
HA	003.9	42.8	103.5	CW	007.9	90	026.8	14.5	80.9	CCW	170.6	90
HD	023.1	39.3	153.1	CW	018.5	90	229.8	35.5	53.8	CW	161.5	90
HU	025.2	48.4	156.7	CW	029.4	90	247.7	37.2	65.7	CW	150.6	90
GD	309.1	67.6	123.6	CW	031.5	90	068.1	16.3	108.1	CCW	148.5	90
MU[*]	324.5	29.5	57.2	CW	144.5	90	002.3	36.7	160.7	CCW	035.5	90

[*] No preferred solution (both solutions are discarded). Results of the net tectonic rotation analysis (Allerton and Vine, 1987) showing the calculated values for the azimuth and plunge of the rotation axis, rotation magnitude and sense, and restored dyke strike and plunge. Reference direction used: D = 000°, I = 21.5° ± 6.6°. In situ dyke orientations and associated uncertainties used for the analysis are in Table 1. Two sets of solutions have been obtained at each site and identified as "preferred" (the one used for the tectonic interpretation) and "alternate" (the one discarded).

giving CW rotations (while the alternate solutions provided CCW rotations). The net tectonic rotation analysis for the remaining four sites DA, FF, HD, and HU yielded CW rotations at both sets of solutions. At sites FF, HD, and HU, the preferred solutions have been selected among those giving the largest vertical-axis rotation (the alternative solutions have shallower axes and smaller net rotations that result in minimum vertical axis rotations, which are incompatible with the large rotation observed regionally). Both solutions at the remaining site DA produce an equal amount of vertical axis rotation, yet the alternate (i.e., rejected) solution together with vertical axis rotation produces overturned units, which is not compatible with the overall gentle tilt of the ophiolite (Nicolas et al., 2000).

Net tectonic rotation analysis at site MU provided two solutions, one of which is clearly meaningless for it gives extremely large CCW rotations. The other set of solutions indicates a CW rotation but the vertical-axis component of this net rotation is quite small and therefore not consistent with the regional large rotation of the ophiolite. Because the *in situ* remanence of site MU is close to the present-day field (Table 1 and Fig. 6) and the tilt corrected directions somewhat in between the directions expected for primarily magnetized and remagnetized rocks, it is indeed likely that this site has been affected by recent remagnetization. We therefore will not consider the result from this site for further analysis.

For the seven localities where preferred solutions were identified we have then modeled the uncertainties associated with the mean paleomagnetic direction, the dyke orientation, and the reference direction (Fig. 7; Table 2). The rotation axes at these seven sites are moderately to steeply plunging approximately to the west (sites AS, FF, and GD), to the north-northeast (sites HA, HU, and HD), and to the southeast (site DA). The rotation magnitude is variable between ∼80° and ∼160°, consistent with the large regional rotation of the ophiolite (Morris et al., 2016). There seems to be no correlation between the orientation of the rotation axes or the magnitude of the net rotations and the location of these seven sites.

The calculated initial dyke strike is consistently NNE to ENE (Table 2 and Fig. 7). When the modeled initial dyke orientations from all seven sites are plotted together (525 directions), the most frequent initial strike of the sheeted dykes at the scale of the whole ophiolite is NNE–SSW, between 020° and 030° (Fig. 7). A bimodal distribution seems to appear in this diagram, with primary NNE–SSW and secondary ENE–WSW directions. We consider the predominant (more frequent) NNE–SSW trend as representative of the direction of the spreading ridge at which these dykes were emplaced in the Cretaceous. The ENE–WSW directions, if meaningful, may be related to dykes locally intruded at an angle to the NNE–SSW trending spreading ridge, or to an artifact of the modeling.

5. Discussion

Our results indicate that the oceanic crust of the Oman ophiolite accreted at a NNE–SSW trending spreading center, which, given the geochemical and geochronological evidence was located in the upper plate above an infant subduction zone (Guilmette et al., 2018; MacLeod et al., 2013; Rioux et al., 2016). Interestingly, regardless of the geochemical signature of the ophiolitic crust, the orientation of this spreading center already makes it quite unlikely that the crust of the Oman ophiolite formed at the Neotethyan mid-oceanic ridge as suggested before (e.g., Nicolas et al., 2000): the overall strike of the Gondwana passive margins, and hence of the Neotethys ridge, was WNW–ESE rather than ∼NNE–SSW (in Cretaceous paleomagnetic coordinates) (Fig. 8b).

The location, in present-day coordinates, of the subduction zone above which the Oman ophiolite was formed is best estimated from the modern obduction front in the western and southern edge of the ophiolite, although post-obduction erosion may have removed some of the most trench-proximal parts of the ophiolite. The sheeted dyke sections strike approximately sub-parallel to this obduction front, suggesting that the spreading occurred orthogonal to the trench. This is further suggested by the narrow, 96–95 Ma age range of the ophiolitic crust along the ophiolite's strike (Rioux et al., 2016). Such a narrow age range is expected when a fast-spreading ridge is located parallel to the subduction front. Upon spreading, this supra-subduction zone ridge migrates away from the trench at half-spreading rate. With spreading rates of 5–10 cm/yr estimated for the Semail ophiolite (Rioux et al., 2016), and an exposed width orthogonal to the obduction front of <100 km, only 1–2 Myr worth of ophiolite spreading history can be preserved in the modern ophiolite, whereas all crust that accreted due to younger spreading must be located offshore northern Oman (Fig. 8d). Had spreading occurred parallel to the trench, the 500 km long ophiolite should have had crustal ages spanning 5–10 Myr from north to south. We therefore conclude that the subduction zone above which the Oman ophiolite accreted was also striking NNE–SSW, parallel to the restored dyke orientation.

A NNE–SSW original orientation of the ophiolite is fully consistent with the vertical axis rotations estimated from paleomagnetic data (Morris et al., 2016) suggesting that the ophiolite underwent up to ∼150° clockwise rotation between the formation of its crust at ∼96–95 Ma, and the end of obduction around 70 Ma (Morris et al., 2016). Back-rotating the ophiolite around its modern northwestern tip to its original NNE–SSW strike provides the minimum horizontal displacement between subduction initiation and obduction. Such a rotation, along a small circle at the ophiolite's southeastern tip, involves a total horizontal motion relative to Arabia of ∼1000 km. This gives an average long-term drift rate of ∼4 cm/yr, which is well within the ranges of similar strongly
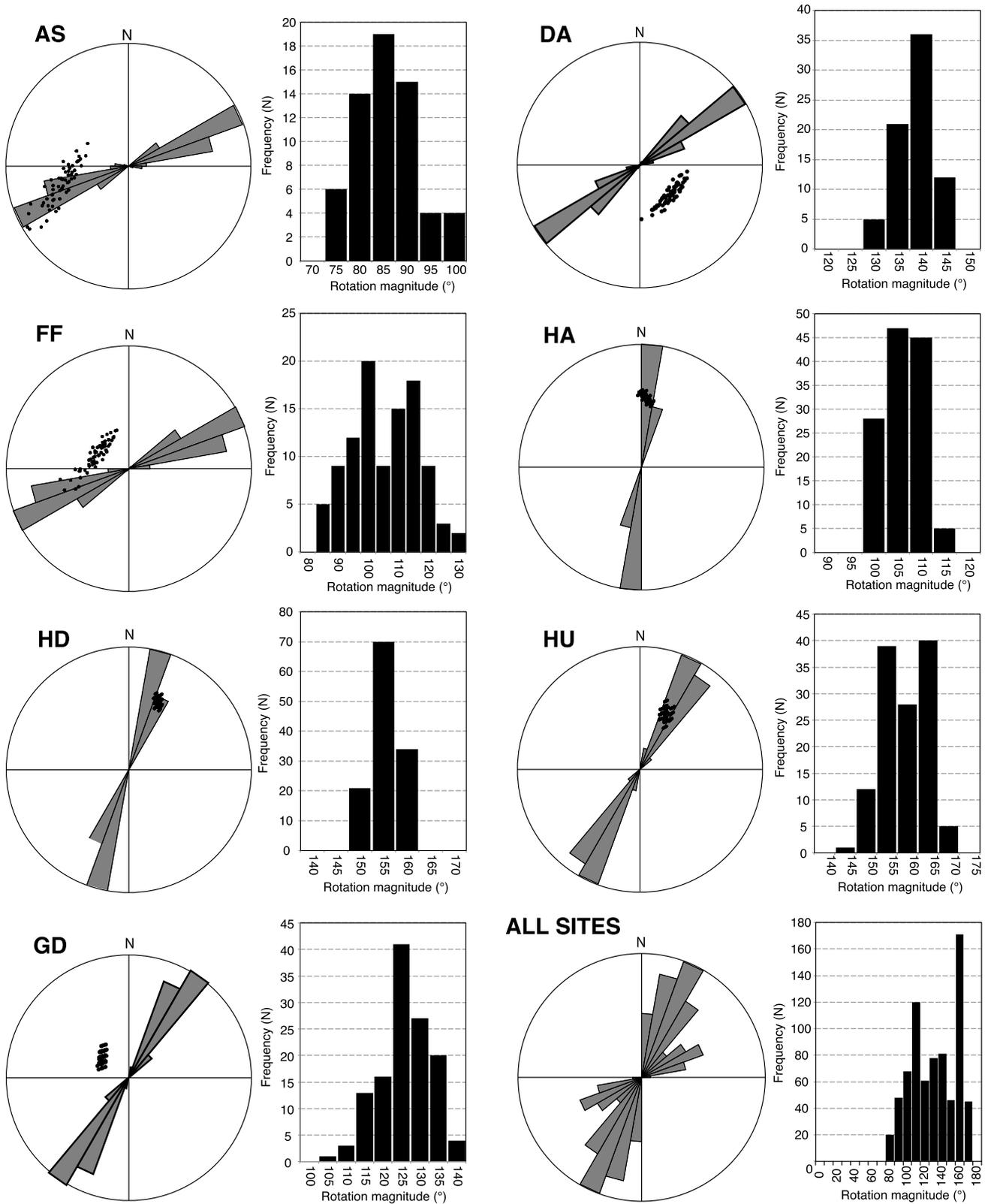
Fig. 7. (Left) Stereographic projections of the permissible initial dyke orientations (rose diagram) and rotation poles calculated after modeling of the uncertainties associated to the input vectors of the net tectonic rotation analysis, following methods of Morris et al. (1998) and Koymans et al. (2016). (Right) Frequency distribution of the permissible rotation magnitude obtained from the same analysis. Summary plots showing the mean initial dyke orientation and rotation magnitude are shown in the bottom right corner, and have been obtained by combining all the permissible results from the seven sites.
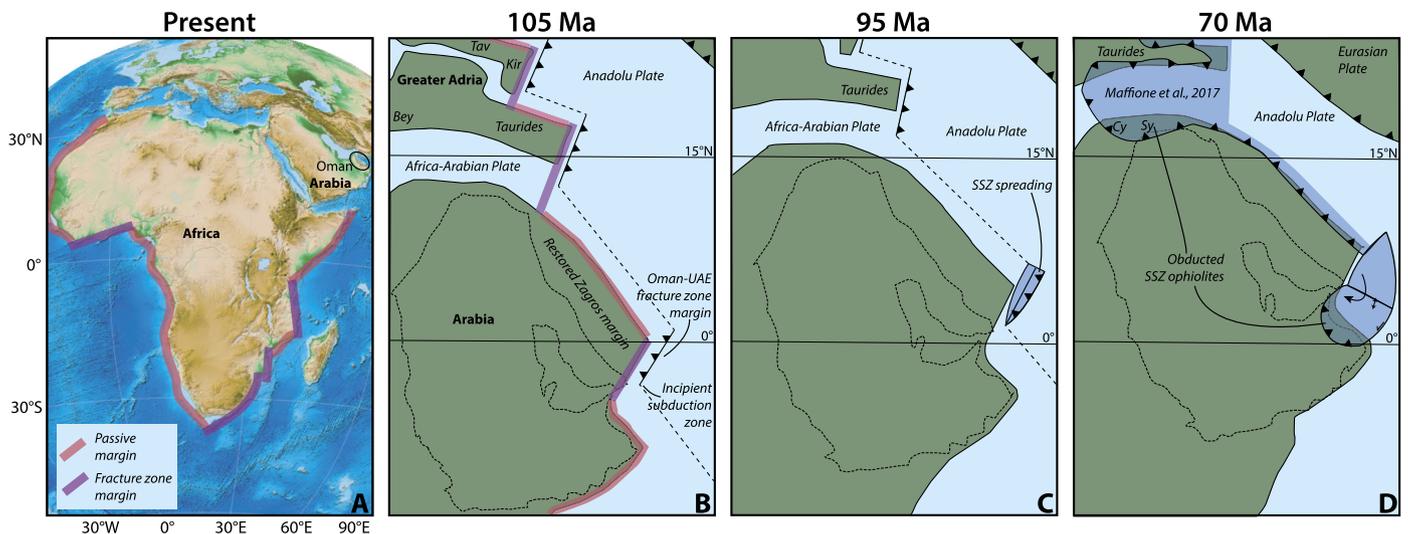
Fig. 8. Tectonic model of subduction initiation along the Arabian margin of Oman. Reconstruction of continents in paleomagnetic reference frame of Torsvik et al. (2012). Reconstruction of the Zagros margin following McQuarrie and van Hinsbergen (2013), and of eastern Mediterranean subduction initiation and obduction following Maffione et al. (2017). A) Fracture zone and passive margins of the modern African continent, providing a modern example of the restored Arabian-Greater Adria continental margin, where the fracture zone margins were the locus of Cretaceous subduction initiation. Basic plate kinematics requires that the N–S subduction segments were connected with a transform fault parallel to (and here dotted along) the Arabian passive margin. B–D) Subduction initiation parallel and close to the Oman-UAE fracture zone margin around 105 Ma is followed by forearc extension around 96–95 Ma, and subsequent rotation of the forearc Oman ophiolite, followed by ∼70 Ma obduction. Bey = Bey Dağları Platform; Kir = Kırşehir Massif, Tav = Tavşanlı Zone; for the tectonic history of the eastern Mediterranean region, see Gürer et al. (2016) and Maffione et al. (2017).

rotating trenches that roll back along and obduct passive margins (e.g., Chertova et al., 2014). This restoration places the ophiolite's northern (i.e. modern eastern) tip at a paleolatitude of ∼5°N. Paleolatitudes calculated from the ophiolite's crust allow for a somewhat more northerly paleolatitude for ophiolite spreading, and the plate motion rates during ophiolite-Arabia convergence may thus have been somewhat higher. Nevertheless, this analysis shows that the ultra-high spreading rates inferred based on U/Pb crustal ages (Rioux et al., 2016) must have been short-lived, focused in the period of inception of upper plate spreading.

Perrin et al. (2000) showed rapid clockwise rotations during ophiolite formation, from major declination differences within the effusive sequence. Whilst the rotation sense and magnitude of these rotations are consistent with the total rotation of the whole ophiolite, the short time span during which the effusive rocks accumulated of only a few million years makes it unlikely that these rotations represent the rotation of the entire ophiolite: if they were representative, these would require plate motion and subduction rates of up to meters per year, which is geodynamically unrealistic. We therefore infer that the results reported in Perrin et al. (2000) reflect tectonic deformation within the ophiolite, e.g. along transform faults, which may cause local rotation, as observed in the Troodos ophiolite of Cyprus (Morris and Maffione, 2016).

Our reconstructed initial trench orientation associated with the Semail ophiolite now allows assessing the nature of the weakness zone at which subduction initiated – the main aim of our study. A NNE–SSW original strike of the subduction zone is approximately orthogonal to the Arabian passive continental margin at ∼95 Ma, when corrected for plate motions in a paleomagnetic reference frame (Torsvik et al., 2012). Weakness zones expected in such an orientation are likely to be fracture zones. This conclusion for the Semail ophiolite does not come in isolation: coeval ophiolites from Cyprus, Syria, and Turkey all share a similar ridge and inferred trench orientation, and also in those settings, trenches and supra-subduction zone ridges were striking N–S to NE–SW, orthogonally to restored passive margins (Maffione et al., 2017) (Fig. 8b). Moreover, such a former fracture zone orientation is preserved in the Arabian margin today along the N–S striking coast of northern Oman and the UAE, connecting passive margins of northeast Oman, and the restored margin of the Zagros mountains in

Iran (Fig. 8b). It thus appears that Cretaceous subduction initiation in the Neotethys Ocean was driven by (ES)E–(WN)W contraction, rather than the widely inferred ∼N–S convergence. This may help in our search for the potential drivers of subduction initiation.

When the underthrusting of the Arabian passive margin at the Zagros collision zone of Iran is restored (McQuarrie and van Hinsbergen, 2013), the original Oman-UAE fracture zone margin, of Permian age (Béchennec et al., 1990; Stampfli and Borel, 2002), extended several hundreds of kilometers farther to the north than today (Fig. 8b). We restore the original orientation of the ophiolite, and of the newly formed subduction zone at which the ophiolite's sole started forming just before 104 Ma, adjacent to this ancient Arabian continent-parallel fracture zone. The initiation probably occurred sufficiently far east of the margin to be in an intra-oceanic setting, since no continental crust relics are found in the ophiolite, but nevertheless close to that continental margin.

Near-continental margin intra-oceanic subduction initiation and formation of supra-subduction zone ophiolites was restored for the Indus-Yarlung ophiolites of southern Tibet (Maffione et al., 2015b). There, it was thus already inferred that supra-subduction zone ophiolites are not necessarily associated with subduction initiation in the vicinity of a mid-ocean ridge. In this study, we propose a similar scenario for the Semail ophiolite, where mid-ocean ridge inversion has long been the preferred model (Boudier et al., 1988; Duretz et al., 2016). Our reconstruction places Arabian lithosphere in the upper plate, but even if subduction initiated farther to the northeast such that oceanic crust adjacent to the Zagros margin was located in the upper plate, it is quite unlikely that an active ridge was present there at that time. Active mid-ocean ridges are commonly not observed in the vicinity of a 170 Myr old passive margin, and as pointed out by Maffione et al. (2017), it is unlikely that the Cretaceous Neotethys ocean between Arabia and Eurasia still contained an active mid-ocean ridge: the ridge at which the Neotethys opened would have long subducted below the Iranian active margin by that time (such as inferred by Stampfli and Borel (2002)). We may thus infer that, in absence of an active mid-ocean ridge in an ocean, passive margins, or fracture zone margins, may be the preferred locus of subduction initiation.

Such settings of continental margin-parallel fracture zones are today abundant along the west and east coast of Africa (Fig. 8a).

Recent studies have shown through seismic interpretation that the fracture zone margin of west Africa was associated with hyper-extension and exhumation of serpentinized mantle during continental breakup (Gillard et al., 2017). Serpentine-rich faults along hyperextended margins are weak and may localize subduction initiation upon forced convergence (Maffione et al., 2015a). We envisage that such a setting may have facilitated subduction initiation in the Oman case, although we note that the old age of this setting at the time of subduction initiation (∼170 Myr) renders it likely that a thick, unbroken lithospheric mantle was present, whose strength must be overcome to initiate subduction.

Our results, and those of Maffione et al. (2017) for the Mediterranean region, raise several first-order new questions for understanding subduction initiation dynamics. Our results show that Cretaceous subduction initiation within the Neotethys ocean formed a new plate (the Anadolu plate of Gürer et al. (2016) separated from Eurasia and Africa-Arabia by trenches (Fig. 8). This plate must have moved westward relative to Africa/Arabia (and Eurasia, given overall N–S Africa-Eurasia convergence) to drive subduction initiation along N–S striking trenches. Gaina et al. (2015) showed based on Indian Ocean reconstructions that prior to the end of the Cretaceous superchron, India rotated counterclockwise relative to Arabia that requires such convergence? Did the driver of this rotation also spark subduction initiation farther westwards? And what processes cause the hot conditions recorded in the Oman metamorphic sole 8 Myr before upper plate spreading (Guilmette et al., 2018) with subduction initiating in old, cold lithosphere? We refrain from speculating on these questions but identify these as key subjects for future study and debate.

6. Conclusions

The subduction zone above which the crust of the Semail ophiolite of Oman formed is widely thought to have initiated along, or in the vicinity of a Neotethyan mid-oceanic ridge. In this paper, we restored the paleo-orientation of the supra-subduction zone ridge at which the Semail ophiolitic crust accreted around ∼96–95 Ma, through paleomagnetic analysis of its sheeted dyke sections. Our results from seven localities covering the entire width of the ophiolite consistently show that this ridge was orientated NNE–SSW. We infer that the trench orientation, marked by the modern obduction front, was oriented sub-parallel to this trench. Our results thus indicate that the trench orientation was approximately orthogonal to the Arabian passive margin. We infer that subduction initiated along a fracture zone that was located parallel to, and likely in the vicinity of, the fracture zone that connected the Permian Arabian passive margin of northern Oman with the margin underthrust below Iran at the Zagros collision zone. This places Arabian continental crust in the upper plate during subduction initiation. Subduction hence did not initiate in the vicinity of the Neotethyan ridge, which according to plate reconstructions had long been subducted during Cretaceous subduction initiation. We conclude that subduction was induced by (ES)E–(WN)W contraction, as previously also inferred for ophiolite belts of the eastern Mediterranean and NW Arabian margins. This may help the future identification of the dynamic trigger of subduction initiation in the Neotethys Ocean.

Acknowledgements

Appendix A. Supplementary material

Supplementary material related to this article can be found online at https://doi.org/10.1016/j.epsl.2019.04.038.

References

Agard, P., Jolivet, L., Vrielynck, B., Burov, E., Monié, P., 2007. Plate acceleration: the obduction trigger? Earth Planet. Sci. Lett. 258, 428–441.

Agard, P., Zuo, X., Funiciello, F., Bellahsen, N., Faccenna, C., Savva, D., 2014. Obduction: why, how and where. Clues from analog models. Earth Planet. Sci. Lett. 393, 132–145.

Agard, P., Yamato, P., Soret, M., Prigent, C., Guillot, S., Plunder, A., Dubacq, B., Chauvet, A., Monié, P., 2016. Plate interface rheological switches during subduction infancy: control on slab penetration and metamorphic sole formation. Earth Planet. Sci. Lett. 451, 208–220.

Allerton, S., Vine, F., 1987. Spreading structure of the Troodos ophiolite, Cyprus: some paleomagnetic constraints. Geology 15, 593–597.

Béchennec, F., Le Métour, J., Rabu, D., Bourdillon-de-Grissac, C., De Wever, P., Beurrier, M.t., Villey, M., 1990. The Hawasina Nappes: stratigraphy, palaeogeography and structural evolution of a fragment of the south-Tethyan passive continental margin. Geol. Soc. (Lond.) Spec. Publ. 49, 213–223.

Boudier, F., Ceuleneer, G., Nicolas, A., 1988. Shear zones, thrusts and related magmatism in the Oman ophiolite: initiation of thrusting on an oceanic ridge. Tectonophysics 151, 275–296.

Chertova, M.V., Spakman, W., Geenen, T., van den Berg, A.P., van Hinsbergen, D.J.J., 2014. Underpinning tectonic reconstructions of the western Mediterranean region with dynamic slab evolution from 3-D numerical modeling. J. Geophys. Res. 119, 5876–5902.

Cowan, R.J., Searle, M.P., Waters, D.J., 2014. Structure of the metamorphic sole to the Oman Ophiolite, Sumeini Window and Wadi Tayyin: implications for ophiolite obduction processes. Geol. Soc. (Lond.) Spec. Publ. 392, 155–175.

Deenen, M.H.L., Langereis, C.G., van Hinsbergen, D.J.J., Biggin, A.J., 2011. Geomagnetic secular variation and the statistics of palaeomagnetic directions. Geophys. J. Int. 186, 509–520.

Dunlop, D.J., Özdemir, Ö., 1997. Rock Magnetism: Fundamentals and Frontiers. Cambridge University Press.

Duretz, T., Agard, P., Yamato, P., Ducassou, C., Burov, E.B., Gerya, T.V., 2016. Thermomechanical modeling of the obduction process based on the Oman Ophiolite case. Gondwana Res. 32, 1–10.

Ernewein, M., Pflumio, C., Whitechurch, H., 1988. The death of an accretion zone as evidenced by the magmatic history of the Sumail ophiolite (Oman). Tectonophysics 151, 247–274.

Feinberg, H., Horen, H., Michard, A., Saddiqi, O., 1999. Obduction-related remagnetization at the base of an ophiolite: paleomagnetism of the Samail nappe lower sequence and of its continental substratum, southeast Oman Mountains. J. Geophys. Res., Solid Earth 104, 17703–17714.

Fisher, R., 1953. Dispersion on a sphere. Proc. R. Soc. Lond. Ser. A, Math. Phys. Sci. 217, 295–305.

Gaina, C., van Hinsbergen, D.J.J., Spakman, W., 2015. Tectonic interactions between India and Arabia since the Jurassic reconstructed from marine geophysics, ophiolite geology, and seismic tomography. Tectonics 34, 875–906.

Gillard, M., Sauter, D., Tugend, J., Tomasi, S., Epin, M.E., Manatschal, G., 2017. Birth of an oceanic spreading center at a magma-poor rift system. Sci. Rep. 7, 15072.

Godard, M., Bosch, D., Einaudi, F., 2006. A MORB source for low-Ti magmatism in the Semail ophiolite. Chem. Geol. 234, 58–78.

Guilmette, C., Smit, M.A., van Hinsbergen, D.J.J., Gürer, D., Corfu, F., Charette, B., Maffione, M., Rabeau, O., Savard, D., 2018. Forced subduction initiation recorded in the sole and crust of the Semail ophiolite, Oman. Nat. Geosci. 11, 688–695.

Gürer, D., van Hinsbergen, D.J.J., Matenco, L., Corfu, F., Cascella, A., 2016. Kinematics of a former oceanic plate of the Neotethys revealed by deformation in the Ulukışla basin (Turkey). Tectonics 35, 2385–2416.

Hacker, B., Mosenfelder, J., Gnos, E., 1996. Rapid emplacement of the Oman ophiolite: thermal and geochronologic constraints. Tectonics 15, 1230–1247.

Hacker, B.R., 1991. The role of deformation in the formation of metamorphic gradients: ridge subduction beneath the Oman ophiolite. Tectonics 10, 455–473.

Hacker, B.R., Gnos, E., 1997. The conundrum of Samail: explaining the metamorphic history. Tectonophysics 279, 215–226.

Hall, C.E., Gurnis, M., Sdrolias, M., Lavier, L.L., Müller, R.D., 2003. Catastrophic initiation of subduction following forced convergence across fracture zones. Earth Planet. Sci. Lett. 212, 15–30.

Kirschvink, J., 1980. The least-squares line and plane and the analysis of palaeomagnetic data. Geophys. J. Int. 62, 699–718.

Koymans, M.R., Langereis, C.G., Pastor-Galán, D., van Hinsbergen, D.J.J., 2016. Paleomagnetism.org: an online multi-platform open source environment for paleomagnetic data analysis. Comput. Geosci. 93, 127–137.

MacLeod, C.J., Lissenberg, J.C., Bibby, L.E., 2013. "Moist MORB" axial magmatism in the Oman ophiolite: the evidence against a mid-ocean ridge origin. Geology 41, 459–462.

Maffione, M., Thieulot, C., van Hinsbergen, D.J.J., Morris, A., Plümper, O., Spakman, W., 2015a. Dynamics of intraoceanic subduction initiation: 1. Oceanic detachment fault inversion and the formation of supra-subduction zone ophiolites. Geochem. Geophys. Geosyst. 16, 1753–1770.

Maffione, M., van Hinsbergen, D.J.J., Koornneef, L.M.T., Guilmette, C., Hodges, K., Borneman, N., Huang, W., Ding, L., Kapp, P., 2015b. Forearc hyperextension dismembered the south Tibetan ophiolites. Geology 43, 475–478.

Maffione, M., van Hinsbergen, D.J.J., de Gelder, G.I.N.O., van der Goes, F.C., Morris, A., 2017. Kinematics of Late Cretaceous subduction initiation in the Neo-Tethys Ocean reconstructed from ophiolites of Turkey, Cyprus, and Syria. J. Geophys. Res., Solid Earth 122, 3953–3976.

McFadden, P., McElhinny, M., 1988. The combined analysis of remagnetization circles and direct observations in palaeomagnetism. Earth Planet. Sci. Lett. 87, 161–172.

McQuarrie, N., van Hinsbergen, D.J.J., 2013. Retrodeforming the Arabia–Eurasia collision zone: age of collision versus magnitude of continental subduction. Geology 41, 315–318.

Morris, A., Maffione, M., 2016. Is the Troodos ophiolite (Cyprus) a complete, transform fault–bounded Neotethyan ridge segment? Geology 44, 199–202.

Morris, A., Anderson, M.W., Robertson, A.H., 1998. Multiple tectonic rotations and transform tectonism in an intraoceanic suture zone, SW Cyprus. Tectonophysics 299, 229–253.

Morris, A., Meyer, M., Anderson, M.W., MacLeod, C.J., 2016. Clockwise rotation of the entire Oman ophiolite occurred in a suprasubduction zone setting. Geology 44, 1055–1058.

Mullender, T.A.T., Frederichs, T., Hilgenfeldt, C., de Groot, L.V., Fabian, K., Dekkers, M.J., 2016. Automated paleomagnetic and rock magnetic data acquisition with an in-line horizontal "2G" system. Geochem. Geophys. Geosyst. 17, 3546–3559.

Nicolas, A., 1989. Structures of Ophiolites and Dynamics of Oceanic Lithosphere. Springer Science & Business Media.

Nicolas, A., Boudier, F., Ildefonse, B., Ball, E., 2000. Accretion of Oman and United Arab Emirates ophiolite–discussion of a new structural map. Mar. Geophys. Res. 21, 147–180.

Pearce, J.A., Lippard, S.J., Roberts, S., 1984. Characteristics and tectonic significance of supra-subduction zone ophiolites. Geol. Soc. (Lond.) Spec. Publ. 16, 77–94.

Perrin, M., Plenier, G., Dautria, J.-M., Cocuaud, E., Prévot, M., 2000. Rotation of the Semail ophiolite (Oman): additional paleomagnetic data from the volcanic sequence. Mar. Geophys. Res. 21, 181–194.

Pourteau, A., Scherer, E.E., Schorn, S., Bast, R., Schmidt, A., Ebert, L., 2019. Thermal evolution of an ancient subduction interface revealed by Lu–Hf garnet geochronology, Halilbağı Complex (Anatolia). Geosci. Front. 10, 127–148.

Rioux, M., Garber, J., Bauer, A., Bowring, S., Searle, M., Kelemen, P., Hacker, B., 2016. Synchronous formation of the metamorphic sole and igneous crust of the Semail

ophiolite: new constraints on the tectonic evolution during ophiolite formation from high-precision U–Pb zircon geochronology. Earth Planet. Sci. Lett. 451, 185–195.

Searle, M., Cox, J., 1999. Tectonic setting, origin, and obduction of the Oman ophiolite. Geol. Soc. Am. Bull. 111.

Searle, M., Warren, C., Waters, D., Parrish, R., 2004. Structural evolution, metamorphism and restoration of the Arabian continental margin, Saih Hatat region, Oman Mountains. J. Struct. Geol. 26, 451–473.

Shelton, A.W., 1984. Geophysical Studies on the Northern Oman Ophiolite. Open University.

Soret, M., Agard, P., Dubacq, B., Plunder, A., Yamato, P., 2017. Petrological evidence for stepwise accretion of metamorphic soles during subduction infancy (Semail ophiolite, Oman and UAE). J. Metamorph. Geol. 35, 1051–1080.

Stampfli, G.M., Borel, G., 2002. A plate tectonic model for the Paleozoic and Mesozoic constrained by dynamic plate boundaries and restored synthetic oceanic isochrons. Earth Planet. Sci. Lett. 196, 17–33.

Stern, R.J., Gerya, T., 2018. Subduction initiation in nature and models: a review. Tectonophysics 746, 173–198.

Stern, R.J., Reagan, M., Ishizuka, O., Ohara, Y., Whattam, S., 2012. To understand subduction initiation, study forearc crust: to understand forearc crust, study ophiolites. Lithosphere 4, 469–483.

Torsvik, T.H., Van der Voo, R., Preeden, U., Mac Niocaill, C., Steinberger, B., Doubrovine, P.V., van Hinsbergen, D.J.J., Domeier, M., Gaina, C., Tohver, E., Meert, J.G., McCausland, P.J.A., Cocks, L.R.M., 2012. Phanerozoic polar wander, palaeogeography and dynamics. Earth-Sci. Rev. 114, 325–368.

van Hinsbergen, D.J.J., Peters, K., Maffione, M., Spakman, W., Guilmette, C., Thieulot, C., Plümper, O., Gürer, D., Brouwer, F.M., Aldanmaz, E., Kaymakcı, N., 2015. Dynamics of intraoceanic subduction initiation: 2. Suprasubduction zone ophiolite formation and metamorphic sole exhumation in context of absolute plate motions. Geochem. Geophys. Geosyst. 16, 1771–1785.

Wakabayashi, J., Dilek, Y., 2003. What constitutes 'emplacement' of an ophiolite?: mechanisms and relationship to subduction initiation and formation of metamorphic soles. Geol. Soc. (Lond.) Spec. Publ. 218, 427–447.

Warren, C.J., Parrish, R.R., Waters, D.J., Searle, M.P., 2005. Dating the geologic history of Oman's Semail ophiolite: insights from U–Pb geochronology. Contrib. Mineral. Petrol. 150, 403–422.

Weiler, P., 2000. Differential rotations in the Oman ophiolite: paleomagnetic evidence from the southern massifs. Mar. Geophys. Res. 21, 195–210.

Zijderveld, J., 1967. AC Demagnetization of Rocks: Analysis of Results, Developments in Solid Earth Geophysics. Elsevier, pp. 254–286.